PHYSICAL REVIEW D **85,** 074016 (2012)

Inclusive charmonium production in the PANDA experiment

A. V. Luchinsky* and S. V. Poslavsky†

Institute for High Energy Physics, Protvino, Russia

(Received 12 November 2011; published 16 April 2012)

The production of the charmonium states in $p\bar{p}$ experiments is considered at the energy rates near the threshold in next to leading order. Such a consideration allows one to obtain nonzero distributions over the transverse momentum of the final charmonium and gives a natural explanation to the existence of the χ_{c1} meson in the final state, which is observed experimentally and cannot be produced in leading order processes. The question of scale dependence of theoretical predictions is discussed.

DOI: 10.1103/PhysRevD.85.074016 PACS numbers: 13.75.−n, 13.60.Le, 14.40.Pq

I. INTRODUCTION

Precision experimental studies of charmonium production in proton-antiproton collisions at low energies is proposed in a new experiment, labeled PANDA [1]. Such studies allow one to obtain a deeper understanding of charmonium physics. The PANDA experiment deals with proton target and antiproton beam energies up to 15 GeV. This energy lies near the charmonium production threshold. In the present article we give theoretical predictions of the inclusive charmonium production in $p\bar{p}$ collisions by accounting for next to leading order diagrams in partonic cross sections. Such an approach was considered by a number of authors [2–7] and applied mainly for proton-proton collisions.

The important part of the PANDA experiment is the detailed analysis of all possible mechanisms of charmonia production. Such an analysis is especially important since at low energies there is significant difference between charmonium production in $p\bar{p}$ and pp. For the pp at low energies the contributions of gluon-gluon, quark-gluon, and quark-antiquark subprocesses are comparable, while for $p\bar{p}$ the quark-antiquark annihilation subprocess dominates. For example, if the energy of the proton beam is equal to 40 GeV, the ratio of ψ production cross sections in $p\bar{p}$ and pp collisions equals $\sigma(p\bar{p})/\sigma(pp) \sim 6$.

Another problem is that the direct production of the ψ meson is suppressed in comparison with the production of the intermediate P-wave states $\chi_{c0,1,2}$ with the subsequent decay $\chi_c \to J/\psi\gamma$. This fact is well confirmed in the experiments [8]. The experimentally observed cross sections of χ_{c2} and χ_{c1} are comparable (the χ_{c0} meson can hardly be observed due to its small radiative width), while the well-known Landau-Yang theorem forbids the formation of the axial meson from two massless gluons. One more difficulty is that the partonic distributions are integrated over the transverse momentum. As a result, such a method does not allow one to obtain the distributions of χ_{c0} and χ_{c2} mesons over p_T.

Initially these problems were solved by the introduction of color-octet components of the quarkonia, which arise naturally in the nonrelativistic QCD, where the expansion over the relative velocity of quarks in the meson is performed. In this model it is assumed that the final meson is formed from a heavy quark pair in a color-octet state that subsequently transforms into a physically observed colorless meson. In the framework of nonrelativistic QCD the probabilities of these transitions are described by the matrix elements of four-fermion operators that are determined from the experimental distributions over the transverse momentum of the final charmonium. We would like to stress, however, that this explanation will not work for charmonium production at lower energies. The reason is that the distributions caused by octet components decrease slowly with the rise of the transverse momentum, but the probability to find such a component in the meson is small, compared with the singlet case. As a result, in the large transverse momentum region the contribution of octet components can be significant, but for small energies and transverse momenta it is suppressed.

Recently another way to solve this problem was proposed, where the so called nonintegrated over the transverse momentum distribution functions $G(x, k_T)$ are used (k_T factorization) [9–11]. In this case both of the above mentioned problems are solved simultaneously. The transverse momentum of the produced in gluon fusion $\chi_{c0,2}$ mesons is explained by the transverse momenta of the initial partons. The axial charmonium meson can also be produced in gluon fusion, since in the framework of k_T factorization gluons have nonzero virtuality of the order k_T^2. There are a number of works that explain the experimental distributions at the Tevatron with the help of these functions (see, for example, [10,12,13]). According to these works, there is no need to introduce color-octet components to reproduce the experimental data on P-wave charmonium p_T distributions. Thus, in the k_T-factorization approach color-singlet components give the main contribution.

Unfortunately, the method, used in the modeling of the unintegrated distribution functions $G(x, k_T)$, is based on the summation of large $\log(1/x)$, so it is not applicable for

*Alexey.Luchinsky@ihep.ru
†stvlpos@mail.ru

low energies, where the gluon momentum fractions are in the range $0.1 < x_g < 0.5$. For this reason we are forced to use the following approximation in our calculations. We start from the collinear gluon distributions with well-known collinear distribution functions. Further we consider the charmonia production at next to leading order in the strong coupling constant α_s. Such a trick enables us to obtain the distributions over p_T for all charmonium states. For χ_{c0} and χ_{c2} production we observe a collinear singularity at $p_T = 0$. To avoid this singularity we introduce a regularization procedure. For directly produced ψ and χ_{c1} such a singularity is absent and we use the whole integration region for p_T.

The next section is devoted to the consideration of different modes of charmonia production and collinear singularity regularization. In the third section we determine the cross sections of the hadronic processes and pay attention to the correct scale parameters choice in $\alpha_s(Q^2)$ and parton distributions $f(x, Q^2)$. Numerical results are also given in Sec. III. The last section is reserved for a brief discussion.

II. PARTONIC SUBPROCESSES

Feynman diagrams corresponding to the charmonium production are presented in Fig. 1. At the leading order [Fig. 1(a)] only processes $gg \to \chi_{c0,2}$ are available. Process $gg \to \psi$ is forbidden by charge parity, while process $gg \to \chi_{c1}$ is forbidden due to the Landau-Yang theorem, which forbids the formation of the axial meson from two massless gluons. Other LO cross sections we give in the Appendix.

Next to leading order diagrams are presented in Figs. 1(b) and 1(c). The first two diagrams in Fig. 1(c) includes the 3-gluon vertex. To avoid delicate problems, bounded with ghost contributions, we recalculated differential cross sections for the process $gg \to Qg$ ($Q = \psi, \chi_{c0,1,2}$) (and also for $qg \to \chi_{0,1,2}q$) in the axial gauge:

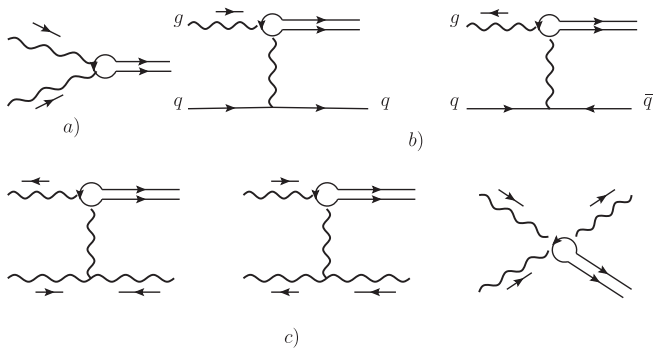

FIG. 1. Feynman diagrams for the charmonium production. (a) Direct $\chi_{c0,2}$ production, (b) through $qg \to \mathcal{Q}q$ and $\bar{q}q \to \mathcal{Q}g$ subprocesses, where $\mathcal{Q} = \chi_{cJ}$, (c) through $gg \to \mathcal{Q}g$ subprocess, where $\mathcal{Q} = \chi_{cJ}$ for the first two diagrams and $\mathcal{Q} = \psi$, χ_{cJ} for the last diagram.

$$\mathcal{L}_{gf} = -\frac{1}{2\xi}(n_\mu A^{a\mu})^2, \tag{1}$$

where n_μ is an auxiliary vector with $n_\mu n^\mu = -1$. This gauge does not require additional ghost Lagrangians, but the gluon propagator and polarization sum becomes more complicated. Using $\xi = 0$ (Landau choice), it can be found that

$$\sum \epsilon_\mu(k)\epsilon_\nu(k) = -\eta_{\mu\nu} + \frac{k_\mu k_\nu}{(k,n)^2} - \frac{k_\mu n_\nu + k_\nu n_\mu}{(k,n)},$$
$$D^{ab}_{\mu\nu}(k) = \delta^{ab}\frac{1}{k^2}\sum \epsilon_\mu(k)\epsilon_\nu(k). \tag{2}$$

The auxiliary vector n_μ will disappear in physical observables. We found that our results are in excellent agreement with [4,5] for the gg channel and [2] for qg channel. Exact formulas for the differential cross sections are rather tedious and can be found in the cited papers.

The massless $\hat{t}$-channel gluon in propagators in Fig. 1 leads to the collinear singularities in small $\hat{t}$ and $\hat{u} = M^2 - \hat{s} - \hat{t}$ regions, where $\hat{s}$, $\hat{t}$, and $\hat{u}$ are the usual Mandelstam variables of the partonic subprocess. For this reason the cross sections of $gg \to \chi_{c0,2}g$ and $qg \to \chi_{c0,2}q$ reactions are divergent:

$$\frac{d\hat{\sigma}}{d\hat{t}} \sim \frac{1}{\hat{t}\,\hat{u}}. \tag{3}$$

In terms of meson transverse momentum $p_T = \sqrt{\hat{t}\,\hat{u}/\hat{s}}$, these singularities correspond to the $p_T \to 0$ singularity. To calculate the total cross section

$$\hat{\sigma}(\hat{s}) = \int_{M^2-\hat{s}}^{\hat{t}} d\hat{t}\frac{d\hat{\sigma}(\hat{s},\hat{t})}{d\hat{t}} = \int_0^{(\hat{s}-M^2)/2\sqrt{\hat{s}}} dp_T \frac{d\hat{\sigma}(\hat{s},p_T)}{dp_T}, \tag{4}$$

some regularization should be performed. The popular decision is to cut off the small p_T region, i.e., restrict the integration region in the last formula by setting $p_T > \Delta$, where the cutoff parameter Δ can be taken from the experimental setup or for some physical reasons. For example, in [2], Δ was taken equal to $1/R_{c\bar{c}}$, where $R_{c\bar{c}}$ is the geometrical size of the charmonium. Such an approach has a big drawback, because the total cross section is highly sensitive to Δ variation. To avoid these difficulties, we will use another regularization procedure.

Taking the indefinite integral of the differential cross section, the following well-known relation can be found:

$$\int d\hat{t}\frac{d\hat{\sigma}(gg \to Qg)}{d\hat{t}} = \frac{\alpha_s}{2\pi}\hat{\sigma}_0(gg \to Q)P_{g\to gg}\left(\frac{M^2}{\hat{s}}\right)\ln\frac{\hat{u}}{\hat{t}} + \text{finite}. \tag{5}$$

Similarly, for the $qg \to Qq$ reaction we have

$$\int d\hat{t}\frac{d\hat{\sigma}(qg\to Qq)}{d\hat{t}} = \frac{\alpha_s}{2\pi}\hat{\sigma}_0(gg\to Q)P_{q\to qg}\left(\frac{M^2}{\hat{s}}\right)\ln\frac{\hat{u}}{\hat{t}} + \text{finite}. \quad (6)$$

In these expressions the second parts are finite when $\hat{t}\to 0$ and $\hat{t}\to M^2-\hat{s}$, while $\hat{\sigma}_0(gg\to Q)$ are given in (A1) and (A2). $P_{g\to gg}(x)$ and $P_{q\to qg}(x)$ are well-known QCD splitting functions:

$$P_{g\to gg}(x) = 6\left(\frac{x}{1-x}+\frac{1-x}{x}+x(1-x)\right)$$
$$P_{q\to qg}(x) = \frac{4}{3}\frac{1+(1-x)^2}{x}.$$

The full hadronic cross section can be obtained by integrating partonic cross sections with partonic distribution functions:

$$\sigma(s) = \int dx_1 dx_2 f(x_1)f(x_2)\hat{\sigma}(\hat{s}). \quad (7)$$

Singular parts of (5) and (6) are included in partonic distribution functions $f(x)$ and generate well-known scaling violations, described by Altarelli-Parisi equations. So inclusion of singular parts in partonic cross sections leads to double counting: one time in $\hat{\sigma}$ and one in $f(x)$. Thus, we will use the regularization

$$\hat{\sigma}^{\text{Reg}}(gg\to Qg) = \left(\int\frac{d\hat{\sigma}(gg\to Qg)}{d\hat{t}}d\hat{t} - \frac{\alpha_s}{2\pi}\hat{\sigma}_0(gg\to Q)P_{g\to gg}\left(\frac{M^2}{\hat{s}}\right)\ln\frac{\hat{u}}{\hat{t}}\right)\Bigg|_{\hat{t}=M^2-\hat{s}}^{\hat{t}=0}, \quad (8)$$

and similarly

$$\hat{\sigma}^{\text{Reg}}(qg\to Qq) = \left(\int\frac{d\hat{\sigma}(qg\to Qq)}{d\hat{t}}d\hat{t} - \frac{\alpha_s}{2\pi}\hat{\sigma}_0(gg\to Q)P_{q\to qg}\left(\frac{M^2}{\hat{s}}\right)\ln\frac{\hat{u}}{\hat{t}}\right)\Bigg|_{\hat{t}=M^2-\hat{s}}^{\hat{t}=0}. \quad (9)$$

In contrast to $\chi_{c0,2}$, differential cross sections for ψ and χ_{c1} have no collinear singularities and are finite at $\hat{t}\to 0$ and $\hat{u}\to 0$. In the case of χ_1, this is explained by the Landau-Yang theorem, which forbids the production from two massless gluons. As a result, the squared matrix element of this reaction is proportional to the virtuality of the intermediate t-channel gluon, so this factor compensates for the divergency, caused by the propagator. For ψ, we have similar reasoning based on charge parity, since the first two diagrams of Fig. 1(c) are absent in this case.

Exact formulas for regularized partonic cross sections are given in the Appendix.

III. HADRONIC CROSS SECTIONS

Let us now consider the full hadronic process

$$A(P_1)B(P_2)\to \mathcal{Q}(P)+X, \quad (10)$$

where A and B are the initial hadrons, $\mathcal{Q}=\psi,\chi_{cJ}$, and in the parentheses corresponding particle momenta are introduced. The cross section of this reaction is expressed through the cross sections of the above considered partonic reactions:

$$\sigma(s) = \sum_{a,b}\int dx_1 dx_2 f_{a/A}(x_1)f_{a/B}(x_2)\hat{\sigma}_{ab}(\hat{s}), \quad (11)$$

where summation is performed over partons a and b, $x_{1,2}$ are the momentum fractions held by these partons, and $f_{a/A}(x_1)$, $f_{b/B}(x_2)$ are the distribution functions of the partons in the initial hadrons. In the common variables

$$x = x_1 - x_2, \quad (12)$$

$$\hat{s} = (x_1P_1 + x_2P_2)^2 = x_1x_2s, \quad (13)$$

the full hadronic cross section becomes

$$\sigma(s) = \sum_{a,b}\int_{M^2}^{s} d\hat{s}\hat{\sigma}_{ab}(\hat{s}) \times \int_{-x(\hat{s})}^{x(\hat{s})}\frac{dx}{\tilde{x}}f_{a/A}(x_1)f_{b/B}(x_2)|_{x_{1,2}=x_{1,2}(x,\hat{s})},$$
$$\tilde{x} = x_1 + x_2, \quad (14)$$

where

$$x(\hat{s}) = 1-\frac{\hat{s}}{s}. \quad (15)$$

In our numerical estimates we used the distribution functions and α_s numeric values presented in the work [14]. Other numerical parameters are equal to

$$M_\psi = 3.097\ \text{GeV}, \qquad M_{\chi_{c0}} = 3.415\ \text{GeV}, \quad (16)$$

$$M_{\chi_{c1}} = 3.511\ \text{GeV}, \qquad M_{\chi_{c2}} = 3.556\ \text{GeV}, \quad (17)$$

$$R_S^2(0) = 0.81\ \text{GeV}^3, \qquad R_P'^2(0) = 0.075\ \text{GeV}^5. \quad (18)$$

A. Scale dependence

There are two physical quantities that depend on some scale choice: parton distributions $f_{a/A}(x,Q^2)$ and the strong coupling constant $\alpha_s(Q^2)$. The parton distribution function $f_{a/A}(x,Q^2)$ gives the probability of finding a parton a of the longitudinal fraction x in physical (anti) proton and transverse momenta $p_T<Q$. It is clear that the exact value of Q depends on parameters of the partonic subprocess, i.e., $Q^2=Q^2(\hat{s})$. It is convenient to set Q^2 to a fixed value Q_*^2-characteristic momentum transfer of the

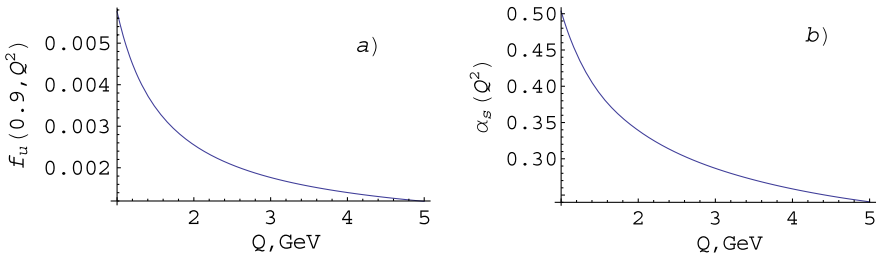

FIG. 2 (color online). (a) Q dependence of u-quark distribution at $x = 0.9$ and (b) Q dependence of α_s.

partonic subprocess. Such a choice can be argued by the mean value theorem, which states

$$\int_a^b f(x)g(x)dx = f(x_*)\int_a^b g(x)dx.$$

On the other hand, from the structure of Altarelli-Parisi equations, it is clear, that at least for high energies ($Q \gg 1$ GeV) the error in choosing Q_* leads to a negligibly small variation of final results; for example, the parton distributions change by $\sim 1\%$ as Q_* is changed by a factor of 10. We have another situation at low energies ($Q \ll 1$ GeV), when perturbation theory works badly, and the error in choosing Q_* leads to a dramatic variation of partonic functions. For example, the u-quark distribution dependence on Q_* is shown in Fig. 2(a).

Second, the physical quantity, depending on some scale choice is $\alpha_s(Q^2)$. Here, the meaning of Q is different from the meaning in distribution functions. The dependence of strong coupling α_s on scale Q occurs when the full propagators and vertices are inserted in tree level diagrams. Similar reasoning, based on the mean value theorem, allows setting $\alpha_s(Q^2)$ to a fixed value with some scale Q_*. The perfect justification of this procedure is given in [15]. Only in the simplest situations can the exact value of Q_* be found; for example, for the $2 \to 2$ reaction through the s-channel particle, it can be found, using the Callan-Symanzik renorm-group equation, that $Q_*^2 = s$. In other cases the exact value of scale can be found only by sequential analysis of perturbation series expansion. It is clear that Q_* depends on the process. At high energies $Q \gg 1$ GeV, $\alpha_s(Q^2)$ becomes almost constant. At the energies' rates near 1 GeV, α_s dependence of Q is shown in Fig. 2(b).

So, in general, we have three possible ways of setting scale parameters in a full cross section:

$$\text{fixed scheme } \sigma(s, Q_*^2) = \sum_{a,b}\int_{M^2}^{s} d\hat{s}\hat{\sigma}_{ab}(\hat{s}, \alpha_s(Q_*^2))\int_{-x(\hat{s})}^{x(\hat{s})}\frac{dx}{\tilde{x}} f_{a/A}(x_1, Q_*^2) f_{b/B}(x_2, Q_*^2),$$

$$\text{float scheme } \sigma(s, Q_*^2) = \sum_{a,b}\int_{M^2}^{s} d\hat{s}\hat{\sigma}_{ab}(\hat{s}, \alpha_s(\hat{s}))\int_{-x(\hat{s})}^{x(\hat{s})}\frac{dx}{\tilde{x}} f_{a/A}(x_1, Q_*^2) f_{b/B}(x_2, Q_*^2),$$

$$\text{float2 scheme } \sigma(s, Q_*^2) = \sum_{a,b}\int_{M^2}^{s} d\hat{s}\hat{\sigma}_{ab}(\hat{s}, \alpha_s(\hat{s}))\int_{-x(\hat{s})}^{x(\hat{s})}\frac{dx}{\tilde{x}} f_{a/A}(x_1, \hat{s}) f_{b/B}(x_2, \hat{s}).$$

The fixed scheme is the most common way used in calculations. The float scheme takes into account the fact that α_s in the partonic subprocess depends on $\hat{s}$. Of course, in general, this dependence is complicated and has the form $\alpha_s(f(\hat{s}))$, but from general considerations it is clear that for a small interval, near process threshold $f(\hat{s}) \sim \hat{s}$. The float2 scheme, takes into account both $\alpha_s(Q^2)$ and $f(x, Q^2)$ scaling. It is also clear that the maximum transverse momentum Q in $f(x, Q^2)$ depends on the $\hat{s}$ and for small energy intervals we set $Q^2 \sim \hat{s}$. Actually, the cross section in the float2 scheme does not depend on Q_*.

In Fig. 3 we show the dependence of the cross section on scheme choice for χ_{c0} production in the $u\bar{u}$ channel at $p\bar{p}$ collisions. It is seen that all three curves are crossed at one point at $Q^2 = M_{\chi_{c0}}^2 = 11.66$ GeV^2. For other mesons and other channels the picture is similar—three curves are crossed at the corresponding squared meson mass. The only exception is the quark-gluon channel, where the cross point is greater at 10% than the corresponding squared meson mass. We make similar calculations for other energy regions and find that these results remain valid. As was expected, at high energies ($s \gg 1$ GeV^2) the difference between schemes is negligible. So these results prove that all schemes are equivalent with the correct Q_* choice:

$$Q_* = M, \tag{19}$$

where M is the corresponding meson mass.

In all further calculations we shall use the fixed scheme with $Q_* = M$.

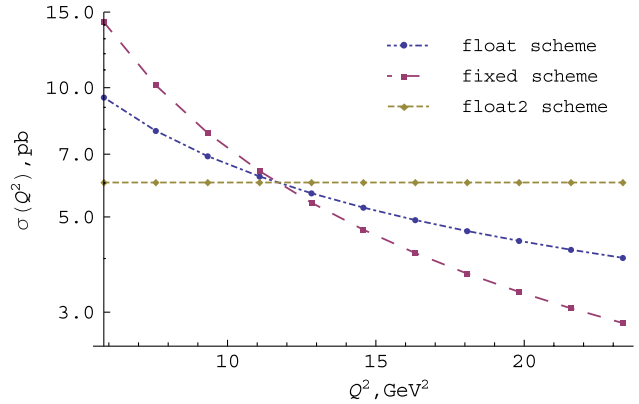

FIG. 3 (color online). Scale dependence in different schemes of the $u\bar{u}$ channel cross section in the $p\bar{p} \to \chi_{c0}X$ collision at the energy $\sqrt{s} = 4.34$ GeV.

B. Total cross sections

Figure 4 illustrates the dependence of ψ production through different processes on total energy. The bold line shows the summed over all processes cross section:

$$\sigma = \sigma_{gg}(\psi) + \mathrm{Br}(\chi_{c0} \to \psi\gamma)\sigma(\chi_{c0}) + \mathrm{Br}(\chi_{c1} \to \psi\gamma)\sigma(\chi_{c1}) + \mathrm{Br}(\chi_{c2} \to \psi\gamma)\sigma(\chi_{c2}), \tag{20}$$

where the branching values are equal to

$$\begin{aligned} \mathrm{Br}(\chi_{c0} \to \psi\gamma) &= 0.016, \\ \mathrm{Br}(\chi_{c1} \to \psi\gamma) &= 0.344, \\ \mathrm{Br}(\chi_{c2} \to \psi\gamma) &= 0.195. \end{aligned} \tag{21}$$

From this picture it is seen that direct ψ production and production from radiative χ_{c0} decay are highly suppressed. The contribution of χ_{c0} radiative decay is negligible, due to very small branching value. As was noted above, the direct ψ production is only available in process $gg \to \psi g$, but the gluon-gluon channel in $p\bar{p}$ reactions is highly suppressed in comparison with the quark-antiquark channel, so the cross section of the direct ψ production is significantly smaller than the production of χ_{cJ}, where the quark-antiquark channel is available.

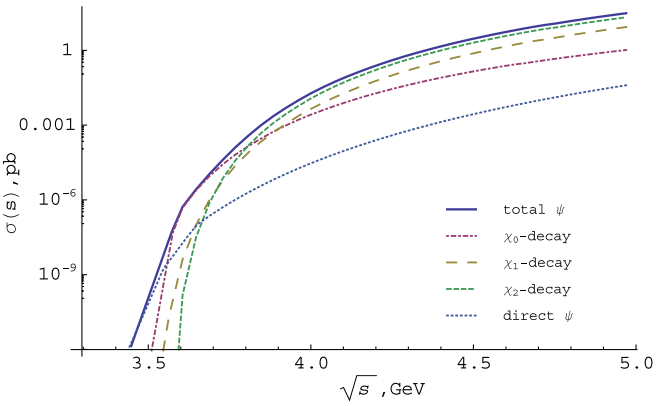

FIG. 4 (color online). Different contributions to the total ψ production in a proton-antiproton reaction for different c.m. energies. (a) Total ψ production, (b) ψ production through the radiative χ_{c2} decay, (c) through the radiative χ_{c1} decay, (d) through the radiative χ_{c0} decay, (e) direct ψ.

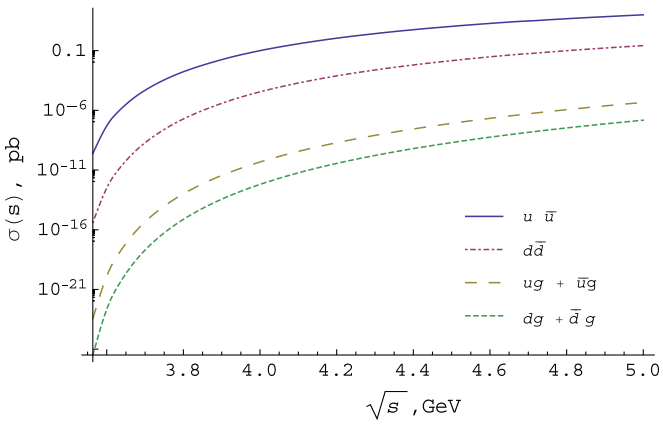

FIG. 5 (color online). Contribution of the different subprocesses to the total χ_{c1} production. (a) $u\bar{u}$ subprocess, (b) $d\bar{d}$ subprocess, (c) the sum over ug and $\bar{u}g$ subprocesses, (d) the sum over dg and $\bar{d}g$ subprocesses.

In Figs. 5 and 6 we show the contributions of the different subprocesses to the total χ_{c1} and χ_{c2} production cross sections. For both mesons the most significant contribution gives the $u\bar{u}$ subprocess. For the gluon-gluon subprocess our numerical results are equal to zero within the error of numerical calculations. The negligibly small effect of the other channels can be easily explained by the structure of the parton distributions. The small energy of the hadronic reaction corresponds to the large longitudinal fraction x. For this region the u-quark distribution function absolutely dominates.

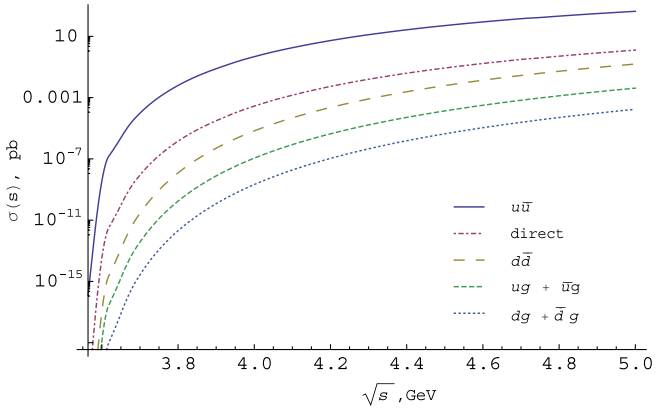

FIG. 6 (color online). Contribution of the different subprocesses to the total χ_{c2} production. (a) $u\bar{u}$ subprocess, (b) direct χ_{c2}, (c) $d\bar{d}$ subprocess, (d) the sum over ug and $\bar{u}g$ subprocesses, (e) the sum over dg and $\bar{d}g$ subprocesses.

C. Production mode at the $s = 32$ GeV^2

It should be stressed that the above presented expressions for charmonia production cross sections can be considered only as estimates on upper bounds. The reason is that in some events initial (anti)protons are present also in the final state. Because of baryonic number conservation in proton-proton scattering this configuration is realized almost always. In proton-antiproton interaction, however, that presence of baryons in the final state is not necessary. Numerically this effect can be described in terms of the inelasticity coefficient, which can be interpreted as the probability of proton-antiproton annihilation into other states. According to [16], this coefficient is equal to $K \sim 0.5$ and decreases slightly with the increase of energy.

If initial baryons are present also in the final state, the effective interaction energy decreases from $\sqrt{s}$ to $\sqrt{s_{\rm eff}} \sim \sqrt{s} - 2M_p$. In the case of high-energy colliders this modification does not change significantly the cross sections of the considered processes. For the PANDA environment, however, the situation is completely different. From Fig. 4 it is clear that the decrease from $\sqrt{s} \sim 5.5$ Gev to $\sqrt{s_{\rm eff}} \sim 3.5$ GeV leads to a dramatic decrease of charmonia production cross sections. So one can expect that the reactions $p\bar{p} \to p\bar{p} + J/\psi + X$ give negligible contributions to the cross sections of charmonia production at PANDA, and expression (14) should be multiplied by the inelasticity factor $K \sim 0.5$.

At the production mode in the PANDA experiment the antiproton beam energy is equal to 15 GeV, which corresponds to the s value equal to 32 GeV^2. The cross section of ψ-meson production is given in (20). Our calculations give

$$\sigma(p\bar{p} \to \psi X) = 0.21 \text{ nb}, \tag{22}$$

where

$$\sigma(p\bar{p} \to \chi_{c1} X) = 0.2 \text{ nb},$$
$$\sigma(p\bar{p} \to \chi_{c2} X) = 0.75 \text{ nb},$$
$$\sigma(p\bar{p} \to \chi_{c0} X) = 0.35 \text{ nb}.$$

The ratio of χ_{c1} and χ_{c2} production cross sections is equal to

$$\frac{\sigma(\chi_{c1})}{\sigma(\chi_{c2})} = 0.26. \tag{23}$$

The p_T distribution of mesons can be obtained by rewriting differential cross sections in terms of $p_T = \sqrt{\hat{t}\,\hat{u}/\hat{s}}$ and integrating with the partonic distributions:

$$\frac{d\sigma}{dp_T} = \int_{(p_T + \sqrt{p_T^2 + M^2})^2}^{s} \frac{d\hat{s}}{s} \frac{d\hat{\sigma}(ab \to \mathcal{Q}c)}{dp_T} \times \int_{-(1-(\hat{s}/s))}^{1-(\hat{s}/s)} \frac{dx}{\tilde{x}} f_{a/A}(x_1) f_{b/B}(x_2), \tag{24}$$

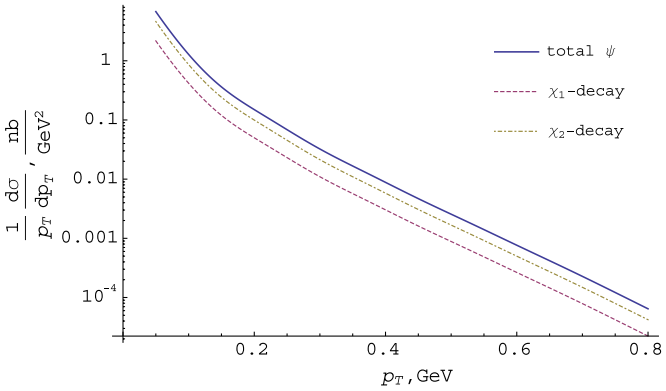

FIG. 7 (color online). Transverse momentum distributions of ψ production with inelasticity coefficient taken into account. (a) Total ψ, (b) ψ production through χ_{c2} decay, (c) ψ production through χ_{c1} decay.

where

$$\frac{d\hat{\sigma}}{dp_T} = \frac{2\hat{s}p_T}{\sqrt{(\hat{s} - M^2)^2 - 4\hat{s}p_T^2}} \left(\frac{d\hat{\sigma}}{d\hat{t}} \bigg|_{\hat{t}=\hat{t}_1} + \frac{d\hat{\sigma}}{d\hat{t}} \bigg|_{\hat{t}=\hat{t}_2} \right),$$
$$\hat{t}_{1,2} = \frac{1}{2}\left(M^2 - \hat{s} \pm \sqrt{(\hat{s} - M^2)^2 - 4\hat{s}p_T^2} \right).$$

As was shown before, the major processes, giving contribution to the total ψ production, are the radiative decays of the $\chi_{c1,2}$ mesons, which in turn are formed through the $u\bar{u}$ subprocess. Thus, for the calculation of the p_T dependence we will neglect all other channels of the ψ production. In this approximation we do not encounter collinear singularities, which appear in other subprocesses of χ_{c2} formation. Another problem arises when we consider the total ψ distribution. The radiative decays $\chi_{cJ} \to \psi\gamma$ can give a significant contribution to the p_T distribution of the final ψ, when the transverse momentum is $\sim$1 GeV. However, we will neglect such a contribution. In Fig. 7 we show the transverse momentum distributions of the ψ production:

$$\frac{d\sigma(\psi)}{dp_T} = \text{Br}(\chi_{c1} \to \psi\gamma) \frac{d\sigma(\chi_{c1})}{dp_T} + \text{Br}(\chi_{c2} \to \psi\gamma) \frac{d\sigma(\chi_{c2})}{dp_T},$$

where

$$\frac{d\sigma(\chi_{c1,2})}{dp_T} = \int \frac{d\hat{s}}{s} \frac{d\hat{\sigma}(u\bar{u} \to \chi_{c1,2} g)}{dp_T} \times \int \frac{dx}{\tilde{x}} f_{u/p}(x_1) f_{\bar{u}/\bar{p}}(x_2).$$

IV. CONCLUSIONS

This paper is devoted to J/ψ-meson production in proton-antiproton interaction at low energies. This process can be used to clarify modes of charmonia production in

hadronic experiments and allows one to measure with higher accuracy proton spectral functions at $x \sim 0.5$.

The physics of charmonia production in hadronic reactions is completely different for different energies. For high-energy experiments (e.g., Tevatron or LHC) heavy quarkonia are produced mainly in the gluon-gluon interaction, since small values of Feynman variable x are allowed kinematically. The contributions of quark-gluon or quark-antiquark modes are negligible. In the threshold region, where only values $x \sim 0.5$ are allowed, on the contrary, main contributions come from quark-gluon (in proton-proton interaction) or quark-antiquark (in the proton-antiproton interactions). In the near future at the FAIR proton-antiproton particle accelerator with $3 < \sqrt{s} < 5.7$ GeV the PANDA detector will perform the first measurements, so a reliable prediction for charmonium meson production for this experiment is required.

In our paper we give predictions for total cross sections of J/ψ-meson production in different modes at next to leading order. The emission of additional gluon leads to nonzero transverse momentum of the final charmonium that is obviously absent in leading order partonic reactions $gg \to \chi_{c0,2}$. It is shown that the main contributions to this process are given by $\chi_{c1,2}$-meson production due to quark-antiquark annihilation with the subsequent radiative decay $\chi_{c1,2} \to J/\psi\gamma$.

Special attention is given to regularization of infrared and collinear singularities in the case of χ_{c2}-meson production, when the t-channel gluon in $gg \to \chi_{c2}g$ partonic reactions leads to divergency in p_T distribution and infinitive values of the cross section.

ACKNOWLEDGMENTS

The authors would like to thank A. K. Likhoded for useful discussions. Also, the authors would like to thank the experimenter's group: V. V. Mochalov, A. N. Vasiliev, and D. A. Morozov for introduction in the PANDA facilities. This research is partially supported by the Russian Foundation for Basic Research (Grant No. 10-02-00061a). The work of A. V. Luchinsky was also supported by the noncommercial foundation Dynasty and the grant of the president of the Russian Federation for young scientists with Ph.D. degree (Grants No. MK-406.2010.2, No. MK-3513.2012.2).

APPENDIX: REGULARIZED PARTONIC CROSS SECTIONS

In this section we give the total cross sections of partonic subprocesses following the procedure described in [17,18]. For subprocesses, in which the collinear singularities appear, we use the regularization procedure, described in the main text.

1. Leading order

In the leading order only $gg \to \chi_{c0,2}$ reactions are possible. The cross sections of these reactions are

$$\hat{\sigma}(gg \to Q) = \hat{\sigma}_0(gg \to Q)\delta(1 - M^2/\hat{s}), \qquad \text{(A1)}$$

where

$$\hat{\sigma}_0(gg \to \chi_0) = 12\frac{\pi^2\alpha_s^2 R'^2_\chi(0)}{M^5\hat{s}},$$
$$\hat{\sigma}_0(gg \to \chi_2) = 16\frac{\pi^2\alpha_s^2 R'^2_\chi(0)}{M^5\hat{s}},$$

where $R'_\chi(0)$ is the derivative of the radial part of the χ-meson wave function at the origin,

2. $gg \to \mathcal{Q}g$

As was noted above, the cross sections for processes $gg \to \psi g$ and $gg \to \chi_{c1}g$ have no collinear singularities, so they do not require regularization. We have

$$\hat{\sigma}(gg \to \psi g) = -\frac{10\pi\alpha_s^3 R_\psi(0)^2}{9\hat{s}^2(M^2-\hat{s})^2(M^2+\hat{s})^3}\Big(M^{10} + 4M^8\hat{s} - 2M^4\hat{s}^3 - M^2\hat{s}^4 - 2M^4\hat{s}(M^4 + 2M^2\hat{s} + 5\hat{s}^2)\log\frac{M^2}{\hat{s}} - 2\hat{s}^5\Big),$$

where $R_\psi(0)$ is the radial part of the ψ-wave function at the origin, and

$$\hat{\sigma}(gg \to \chi_1 g) = \frac{4\pi\alpha_s^3 R'^2_\chi(0)}{M^7\hat{s}^2(M^2-\hat{s})^4(M^2+\hat{s})^5}\Big(12M^4\hat{s}(M^{16} + 9M^{14}\hat{s} + 26M^{12}\hat{s}^2 + 28M^{10}\hat{s}^3 + 17M^8\hat{s}^4 + 7M^6\hat{s}^5 - 40M^4\hat{s}^6 - 4M^2\hat{s}^7 - 4\hat{s}^8)\log\frac{M^2}{\hat{s}} - (M^2-\hat{s})(M^2+\hat{s})(M^{18} + 39M^{16}\hat{s} + 145M^{14}\hat{s}^2 + 251M^{12}\hat{s}^3 + 119M^{10}\hat{s}^4 - 153M^8\hat{s}^5 - 17M^6\hat{s}^6 - 147M^4\hat{s}^7 - 8M^2\hat{s}^8 + 10\hat{s}^9)\Big).$$

The gg production of $\chi_{c0,2}$ states has collinear singularities. Performing the regularization procedure (8), we obtain

$$\hat{\sigma}^{\mathrm{Reg}}(gg \to \chi_0 g) = -\frac{2\pi\alpha_s^3 R'^2_\chi(0)}{3M^7\hat{s}^3(M^2-\hat{s})^4(M^2+\hat{s})^5}\Big(99M^{24} + 132M^{22}\hat{s} - 7M^{20}\hat{s}^2 - 80M^{18}\hat{s}^3 + 210M^{16}\hat{s}^4 - 560M^{14}\hat{s}^5 + 802M^{12}\hat{s}^6 + 696M^{10}\hat{s}^7 - 1721M^8\hat{s}^8 - 244M^6\hat{s}^9 + 789M^4\hat{s}^{10} + 56M^2\hat{s}^{11} + 12\hat{s}(-24M^{22} - 41M^{20}\hat{s} + 10M^{18}\hat{s}^2 + 7M^{16}\hat{s}^3 + 42M^{14}\hat{s}^4 - 176M^{12}\hat{s}^5 - 10M^{10}\hat{s}^6 + 40M^8\hat{s}^7 + 14M^6\hat{s}^8 - 31M^4\hat{s}^9 + 9\hat{s}^{11})\log\frac{M^2}{\hat{s}} - 172\hat{s}^{12}\Big),$$

$$\hat{\sigma}^{\mathrm{Reg}}(gg \to \chi_2 g) = -\frac{4\pi\alpha_s^3 R'^2_\chi(0)}{3M^7\hat{s}^3(M^2-\hat{s})^4(M^2+\hat{s})^5}\Big(66M^{24} + 201M^{22}\hat{s} - 31M^{20}\hat{s}^2 - 728M^{18}\hat{s}^3 + 360M^{16}\hat{s}^4 - 266M^{14}\hat{s}^5 + 256M^{12}\hat{s}^6 + 1032M^{10}\hat{s}^7 - 752M^8\hat{s}^8 - 271M^6\hat{s}^9 + 207M^4\hat{s}^{10} + 32M^2\hat{s}^{11} - 12\hat{s}(12M^{22} + 5M^{20}\hat{s} + 17M^{18}\hat{s}^2 + 86M^{16}\hat{s}^3 - 204M^{14}\hat{s}^4 + 11M^{12}\hat{s}^5 + 31M^{10}\hat{s}^6 + 74M^8\hat{s}^7 - 8M^6\hat{s}^8 + 22M^4\hat{s}^9 - 6\hat{s}^{11})\log\frac{M^2}{\hat{s}} - 106\hat{s}^{12}\Big).$$

3. $qg \to \mathcal{Q}q$

At the qg channel only the χ_{cJ} mesons can be produced. The χ_1-meson cross section does not require regularization and is equal to

$$\hat{\sigma}(qg \to \chi_1 q) = \frac{16\pi\alpha_s^3 R'^2_\chi(0)}{9M^7\hat{s}^3}\Big(4M^6 - 9M^2\hat{s}^2 + 3M^4\hat{s}\log\frac{\hat{s}}{M^2} + 5\hat{s}^3\Big). \tag{A2}$$

Regularized cross sections for $\chi_{c0,2}$ are

$$\hat{\sigma}^{\mathrm{Reg}}(qg \to \chi_0 q) = -\frac{16\pi\alpha_s^3 R'^2_\chi(0)}{27M^7\hat{s}^3}\Big(4M^6 - 18M^4\hat{s} + 57M^2\hat{s}^2 + 3\hat{s}(4M^4 - 9M^2\hat{s} + 9\hat{s}^2)\log\frac{M^2}{\hat{s}} - 43\hat{s}^3\Big),$$

$$\hat{\sigma}^{\mathrm{Reg}}(qg \to \chi_2 q) = -\frac{16\pi\alpha_s^3 R'^2_\chi(0)}{27M^7\hat{s}^3}\Big(20M^6 - 36M^4\hat{s} + 69M^2\hat{s}^2 + 3\hat{s}(5M^4 - 12M^2\hat{s} + 12\hat{s}^2)\log\frac{M^2}{\hat{s}} - 53\hat{s}^3\Big).$$

4. $q\bar{q} \to Qg$

At the $q\bar{q}$ channel, all cross sections are finite. This is explained by the fact that their differential cross sections are cross-symmetric ($\hat{t} \leftrightarrow \hat{s}$) to the qg ones,

$$|\mathcal{M}(qg \to Qq)|^2 = |\mathcal{M}(q\bar{q} \to Qg)|^2|_{\hat{t}\leftrightarrow\hat{s}}, \tag{A3}$$

and the total cross sections are

$$\hat{\sigma}(q\bar{q} \to \chi_0 g) = -\frac{128\pi\alpha_s^3 R'^2_\chi(0)}{81M^3\hat{s}^3(M^2-\hat{s})}(\hat{s}-3M^2)^2, \tag{A4}$$

$$\hat{\sigma}(q\bar{q} \to \chi_2 g) = -\frac{256\pi\alpha_s^3 R'^2_\chi(0)}{81M^3\hat{s}^3(M^2-\hat{s})}(6M^4 + 3M^2\hat{s} + \hat{s}^2), \tag{A5}$$

$$\hat{\sigma}(q\bar{q} \to \chi_1 g) = -\frac{256\pi\alpha_s^3 R'^2_\chi(0)}{27M^3 s^2(M^2-s)}(M^2+s). \tag{A6}$$

[1] PANDA Collaboration, arXiv:0903.3905.
[2] A. K. Likhoded and A. V. Luchinsky, Phys. At. Nucl. **71**, 294 (2008).
[3] R. Baier and R. Ruckl, Phys. Lett. **102B**, 364 (1981).
[4] R. Gastmans, W. Troost, and T. T. Wu, Nucl. Phys. **B291**, 731 (1987).
[5] M. M. Meijer, J. Smith, and W. L. van Neerven, Phys. Rev. D **77**, 034014 (2008).
[6] V. G. Kartvelishvili, A. K. Likhoded, and S. R. Slabospitsky, Sov. J. Nucl. Phys. **28**, 678 (1978).
[7] S. S. Gershtein, A. K. Likhoded, and S. R. Slabospitsky, Sov. J. Nucl. Phys. **34**, 128 (1981).

[8] T. Alexopoulos *et al.* (E771 Collaboration), Phys. Rev. D **62**, 032006 (2000).
[9] O. Teryaev and A. Tkabladze, Phys. Rev. D **56**, 7331 (1997).
[10] B. A. Kniehl, D. V. Vasin, and V. A. Saleev, Phys. Rev. D **73**, 074022 (2006).
[11] S. P. Baranov, Phys. Rev. D **73**, 074021 (2006).
[12] P. Hagler, R. Kirschner, A. Schafer, L. Szymanowski, and O. V. Teryaev, Phys. Rev. Lett. **86**, 1446 (2001).
[13] A. K. Likhoded, V. A. Saleev, and D. V. Vasin, Phys. At. Nucl. **69**, 94 (2006).
[14] S. Alekhin, Phys. Rev. D **68**, 014002 (2003).
[15] J. Stanley Brodsky, G. Peter Lepage, and B. Paul Mackenzie, Phys. Rev. D **28**, 228 (1983).
[16] L.-K. Ding andQ.-Q. Zhu, Phys. Lett. B **297**, 201 (1992).
[17] E. L. Berger and D. L. Jones, Phys. Rev. D **23**, 1521 (1981).
[18] E. Braaten and J. Lee, Phys. Rev. D **67**, 054007 (2003).